iScience, Volume *23*

Supplemental Information

Efficient Photoelectron Capture by Ni Decoration in *Methanosarcina barkeri*-CdS Biohybrids for Enhanced Photocatalytic CO_2-to-CH_4 Conversion

Jie Ye, Guoping Ren, Li Kang, Yiyun Zhang, Xing Liu, Shungui Zhou, and Zhen He

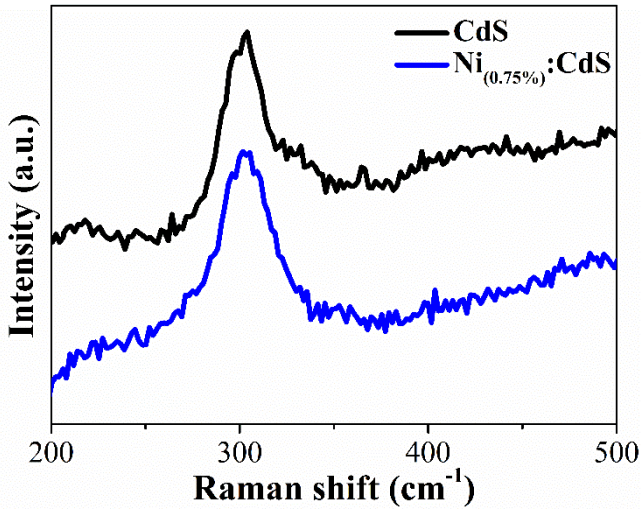

Fig. S1 The Cd-S (at 200-350 cm^{-1}) single cell Raman mapping of pure CdS and $Ni_{(0.75\%)}$:CdS nanoparticles. Related to Figure 1.

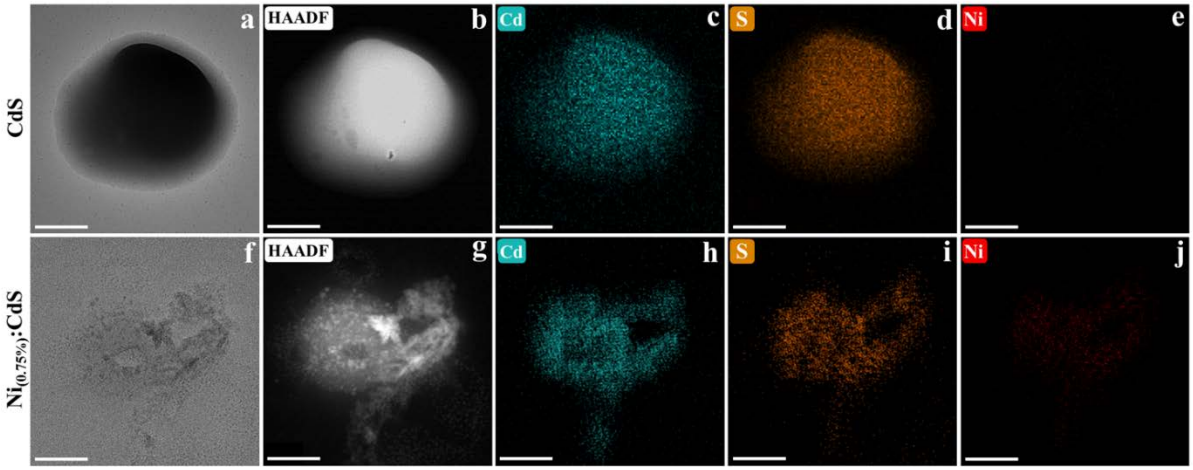

Fig. S2 TEM images (**a** and **f**), High-angle annular dark field (HAADF) images (**b** and **g**), and elements formed by Cd (**c** and **h**), S (**d** and **i**) and Ni (**e** and **j**) with EDS mapping of pure CdS and $Ni_{(0.75\%)}$:CdS semiconductors. The scale bars are 100 nm. Related to Figure 1.

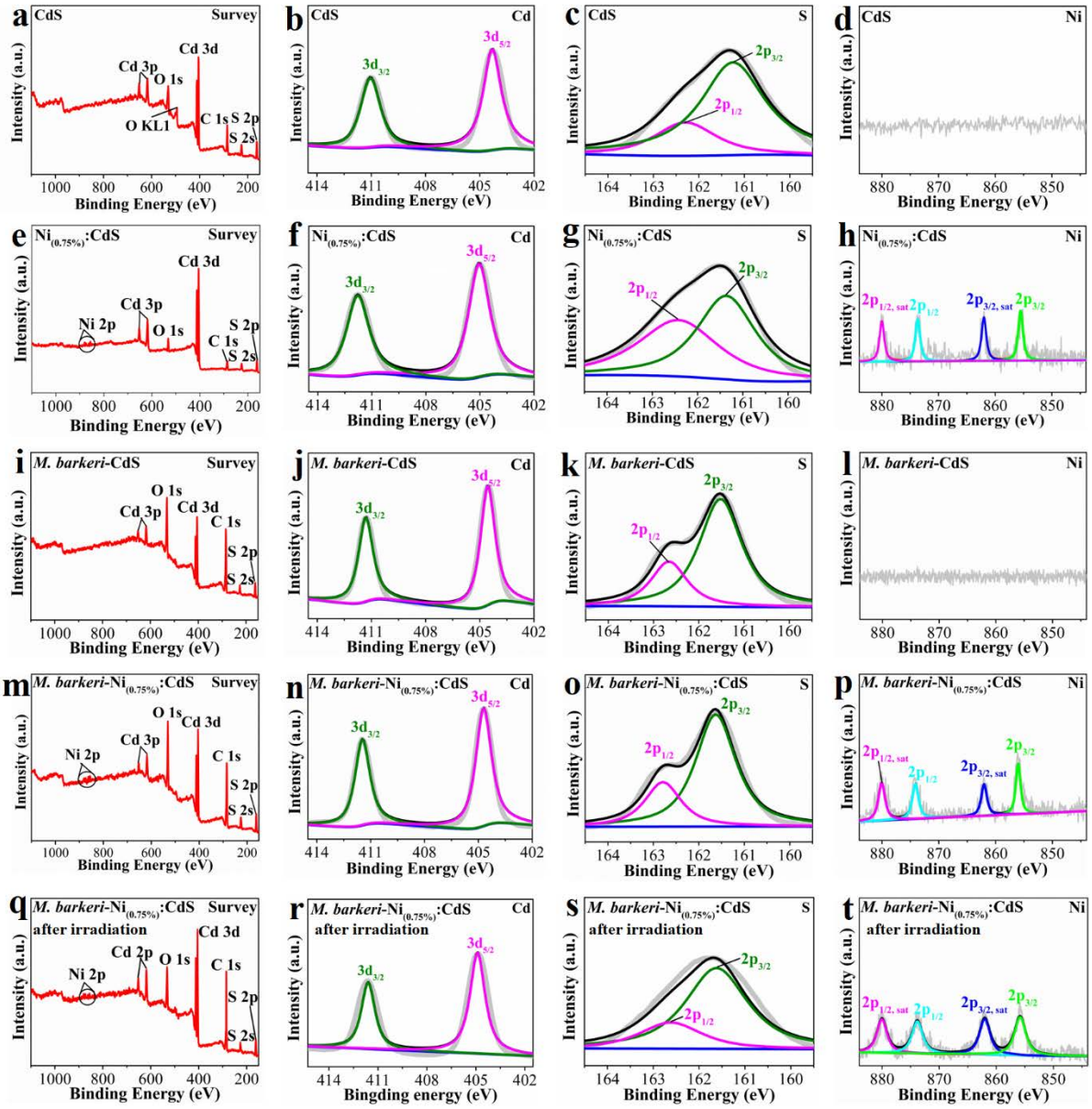

Fig. S3 XPS spectra of pure CdS semiconductor (**a-d**), pure $Ni_{(0.75\%)}$:CdS semiconductor (**e-h**), *M. barkeri*-CdS biohybrids (**i-l**), *M. barkeri*-$Ni_{(0.75\%)}$:CdS biohybrids (**m-p**) and *M. barkeri*-$Ni_{(0.75\%)}$:CdS biohybrids after irradiation (**q-t**). Related to Figure 1.

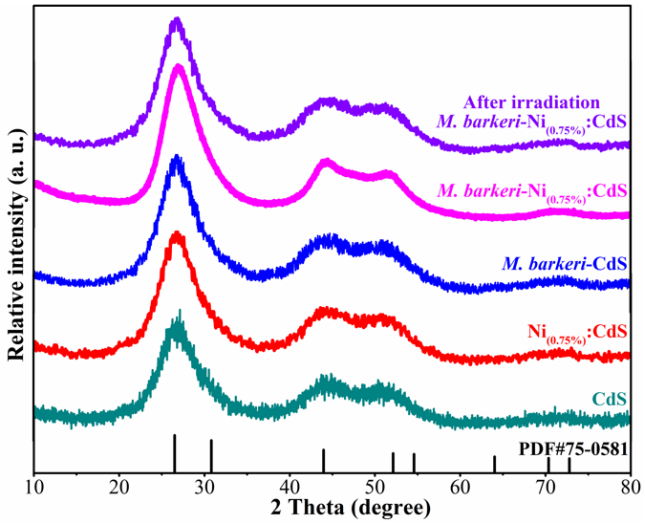

Fig. S4 X-Ray Diffraction patterns of pure CdS semiconductor, pure $Ni_{(0.75\%)}$:CdS semiconductor, *M. barkeri*-CdS biohybrids, *M. barkeri*-$Ni_{(0.75\%)}$:CdS biohybrids and *M. barkeri*-$Ni_{(0.75\%)}$:CdS biohybrids after irradiation. (reference peak from JCPDS data card No. 75-0581). Related to Figure 1.

The prepared semiconductors exhibited similar diffraction patterns, three distinct diffraction peaks at 26.7°, 44.1°, and 52.2°, which could be attributed to the (111), (220), and (311) crystal planes of CdS (JCPDS No. 75-0581), respectively. No peaks of any other impurities were detected, demonstrating the possible formation of pure CdS semiconductors. Meanwhile, The SEM and HRTEM images further indicated that almost no amorphous by-products formed during the preparation of $Ni_{(0.75\%)}$:CdS semiconductor. The fringes with d values of 0.35 nm, 0.21 nm and 0.18 nm could be attributed to the (111), (220), and (311) crystal planes of CdS, respectively.

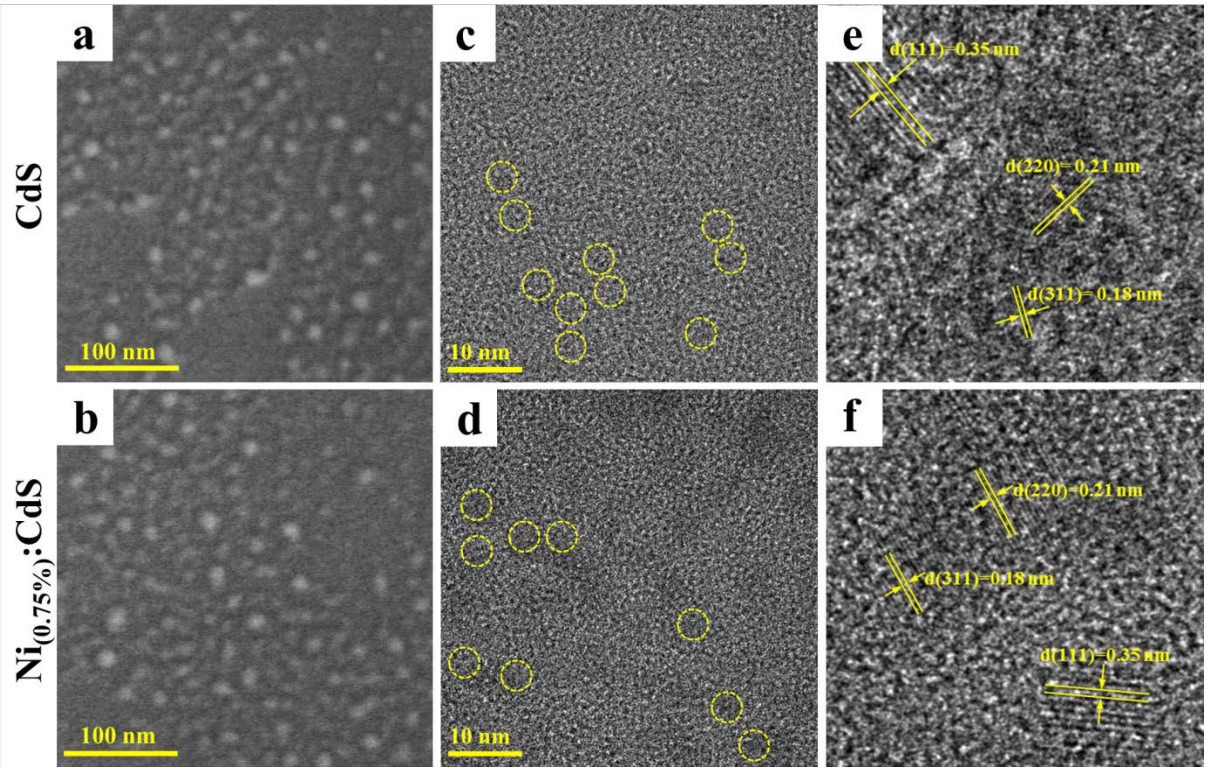

Fig. S5 The SEM images of pure CdS (**a**) and $Ni_{(0.75\%)}$:CdS (**b**) semiconductors, the high resolution TEM (HRTEM) images of pure CdS (**c**, **e**) and $Ni_{(0.75\%)}$:CdS semiconductors (**d, f**). Related to Figure 1.

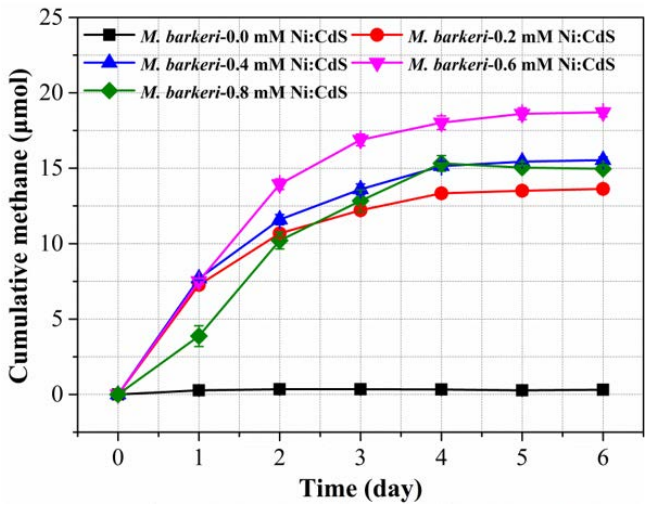

Fig. S6 Effect of different dosages on the CH_4 production performance of *M. barkeri*-$Ni_{(x)}$:CdS biohybrids. Data are represented as mean ± SEM (n = 3). Related to Figure 1.

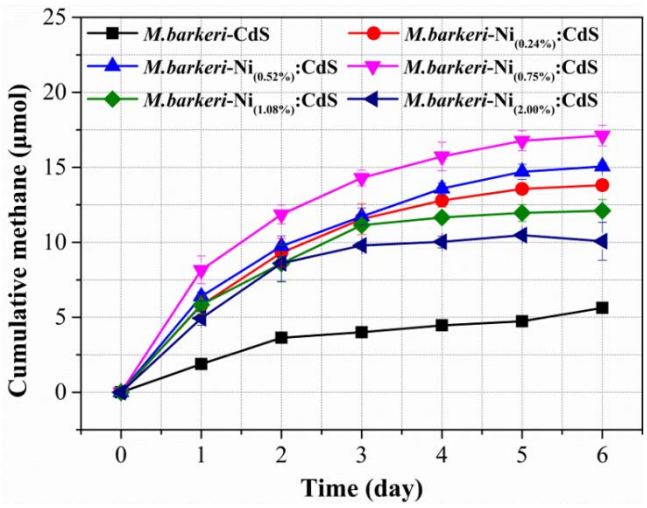

Fig. S7 Effect of different Ni weight ratios (0.24%, 0.52%, 0.75%, 1.08%, and 2.00%) on the CH_4 production performance of *M. barkeri*-$Ni_{(x)}$:CdS biohybrids. Data are represented as mean ± SEM (n = 3). Related to Figure 1.

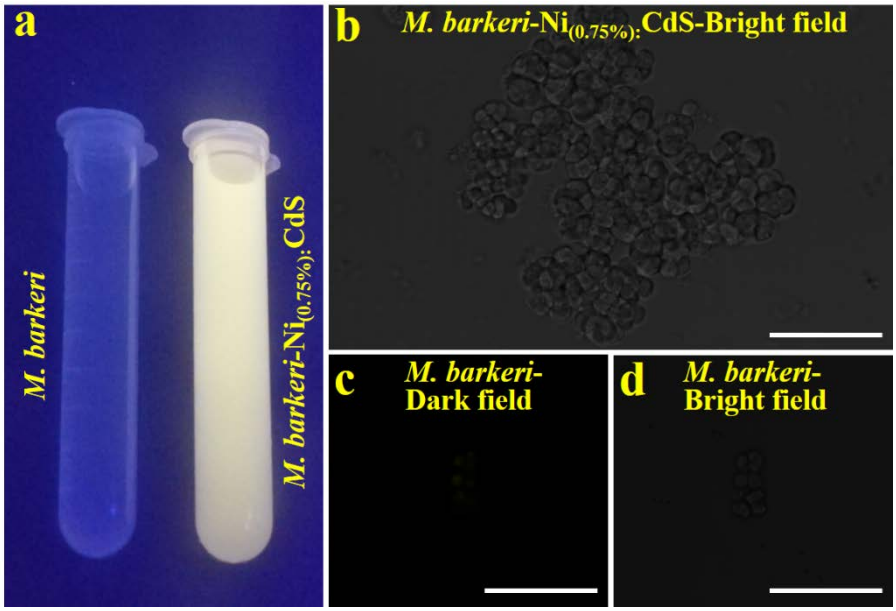

Fig. S8 Fluorescence of *M. barkeri* and *M. barkeri*-$Ni_{(0.75\%)}$:CdS under UV irradiation (a); Confocal laser-scanning microscopic image of *M. barkeri*-$Ni_{(0.75\%)}$:CdS with bright field (b); Confocal laser scanning microscopic images of *M. barkeri* with dark (c) and bright field (d) under 410 nm. All the scale bar are 20 μm. Related to Figure 1.

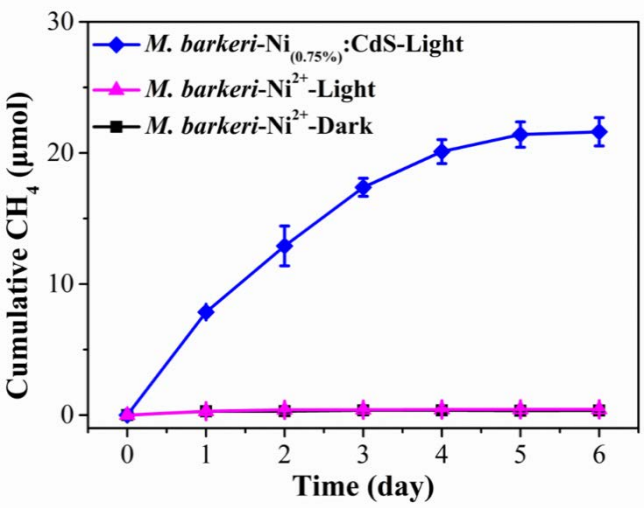

Fig. S9 The CH_4 production by *M.barkeri*-Ni^{2+}-Light and *M. barkeri*-Ni^{2+}-Dark controls with the addition of the same Ni^{2+} as that in *M. barkeri*-$Ni_{(0.75\%)}$:CdS biohybrids. Data are represented as mean ± SEM (n = 3). Related to Figure 2.

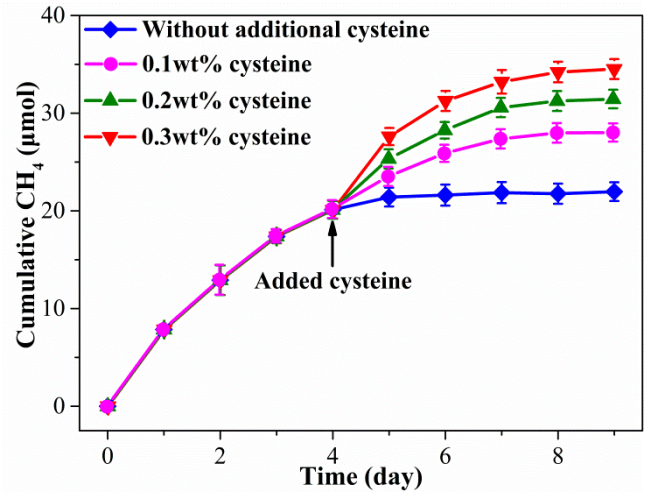

Fig. S10 Cys-dependent CH_4 yield by *M. barkeri*-$Ni_{(0.75\%)}$:CdS biohybrids with Cys added after 4 days of irradiation, for additional 5 days of photosynthesis. Data are represented as mean ± SEM (n = 3). Related to Figure 2.

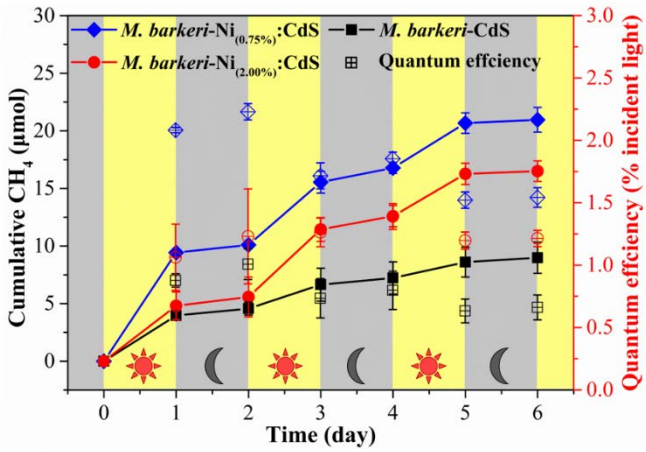

Fig. S11 Cumulative CH_4 and quantum efficiency of different biohybrids with a light-dark cycle of 1 day. Data are represented as mean ± SEM (n = 3). Related to Figure 2.

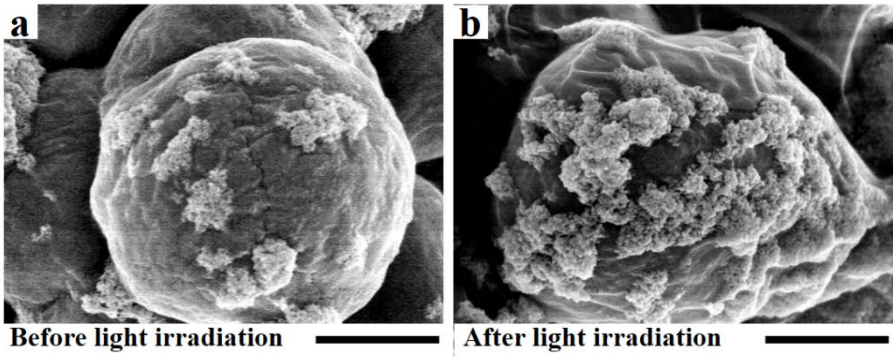

Fig. S12 SEM images of photooxidative damage to *M. barkeri*-Ni(0.75%):CdS biohybrids with the light intensity of 1.6 mW/cm^2. All scale bars are 1 μm. Related to Figure 2.

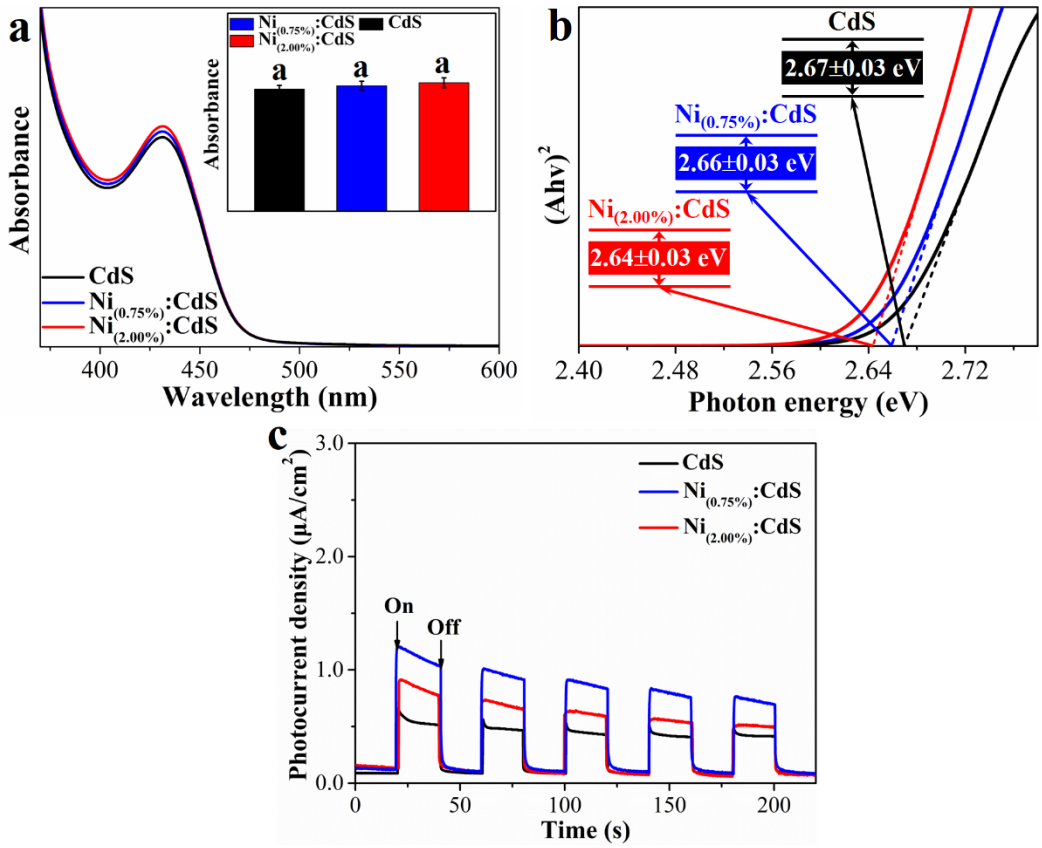

Fig. S13 UV-vis adsorption spectra (**a**), Tauc plots (**b**) and *I-t curve* (**c**) of pure CdS, $Ni_{(0.75\%)}$:CdS and $Ni_{(2.00\%)}$:CdS semiconductors. Related to Figure 3.

Although previous research demonstrated that the metal Ni might be a promising plasmonic promoter (Pei et al., 2019; Meng et al., 2014), no significant difference in the absorption intensity between CdS and $Ni_{(x)}$:CdS nanoparticles (Fig. S16), particularly in the visible light region (> 530 nm), demonstrating that no obvious plasmonic effect was performed after loading Ni atoms to CdS semiconductors. Data are represented as mean ± SEM (n = 3).

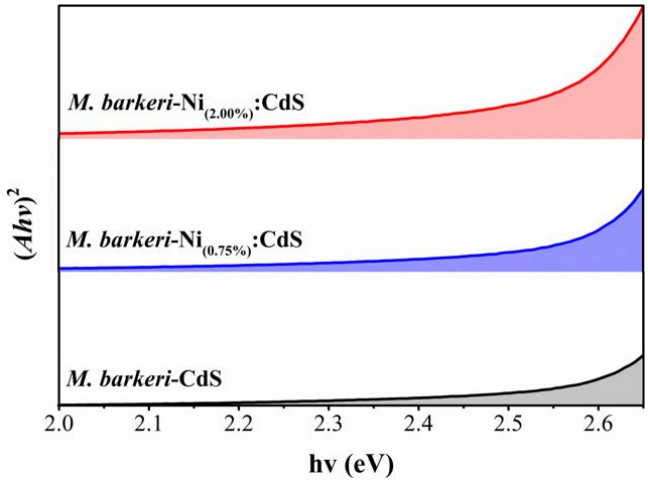

Fig. S14 Plots of $(Ahv)^2$ versus the energy of exciting light (hv) for 2.0~2.65 eV. Related to Figure 3.

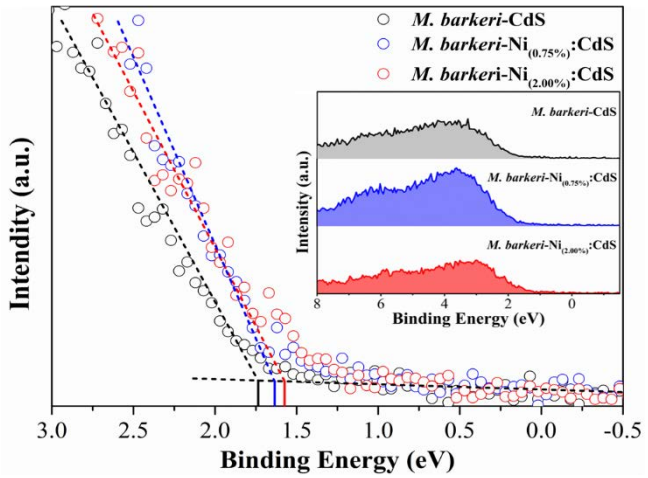

Fig. S15 Valence band XPS spectra of different biohybrids. Related to Figure 3.

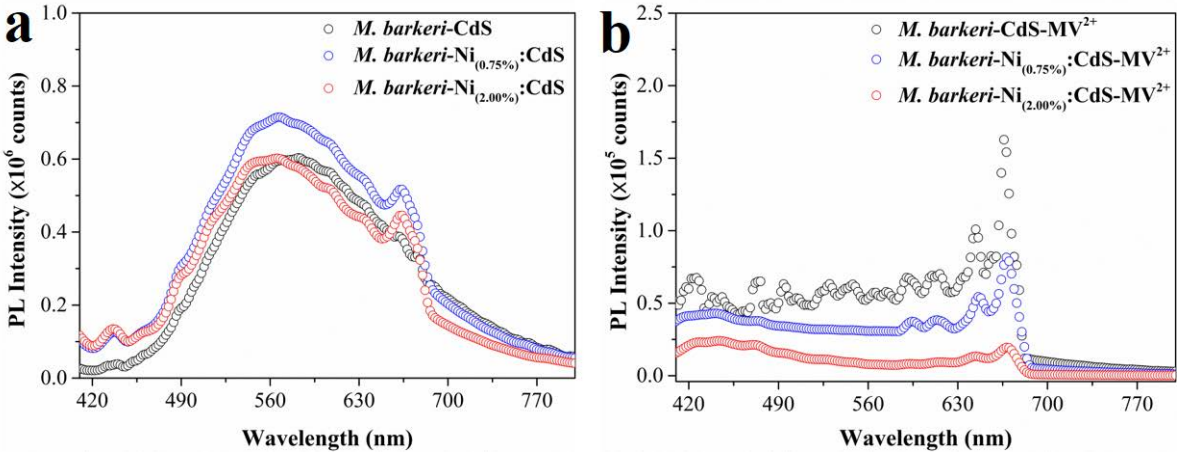

Fig. S16 PL emission spectra of three treatments in the absence (a) and presence (b) of 10^{-5} M MV^{2+} (λ_{ex} = 380 nm). Related to Figure 3.

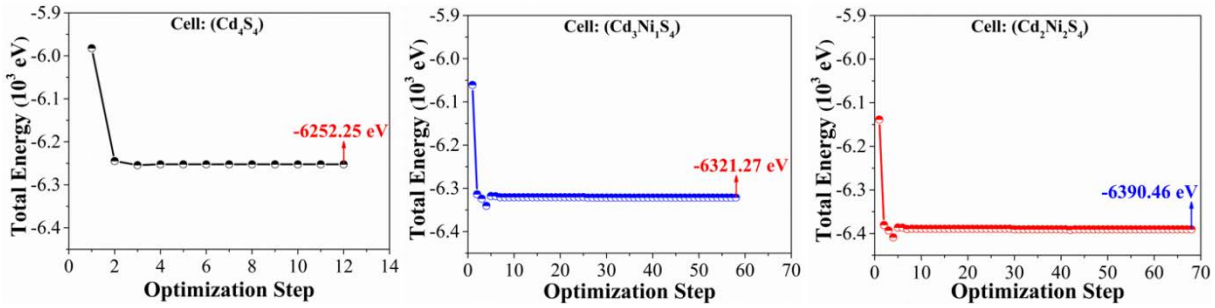

Fig. S17 Corresponding total energy evolution during geometry optimization process. Related to Figure 4.

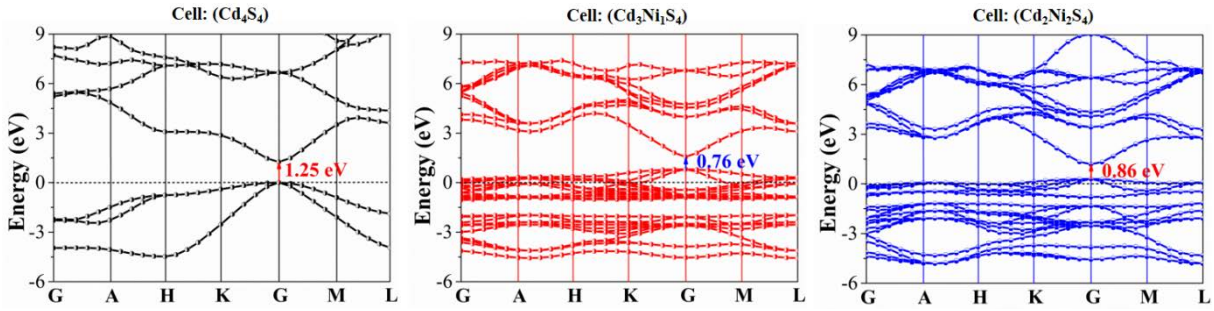

Fig. S18 Band structure plots of the simulated Ni:CdS systems. Related to Figure 4.

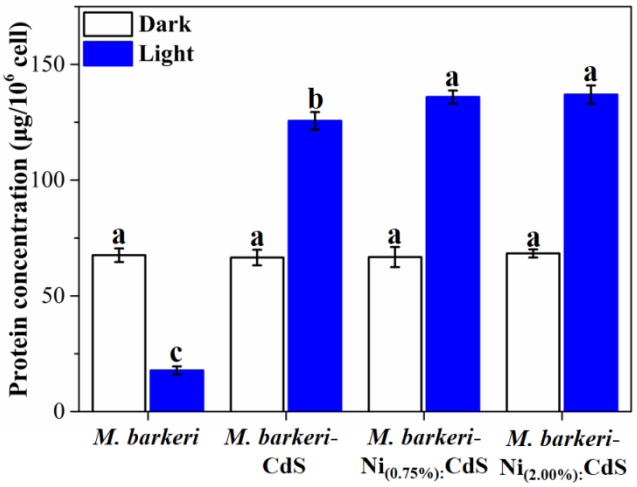

Fig. S19 Concentrations of membrane-bound protein based on the normalization results. Data are represented as mean ± SEM (n = 3), and the different letters represented statistically significant difference ($p < 0.05$) in different groups. Related to Figure 5.

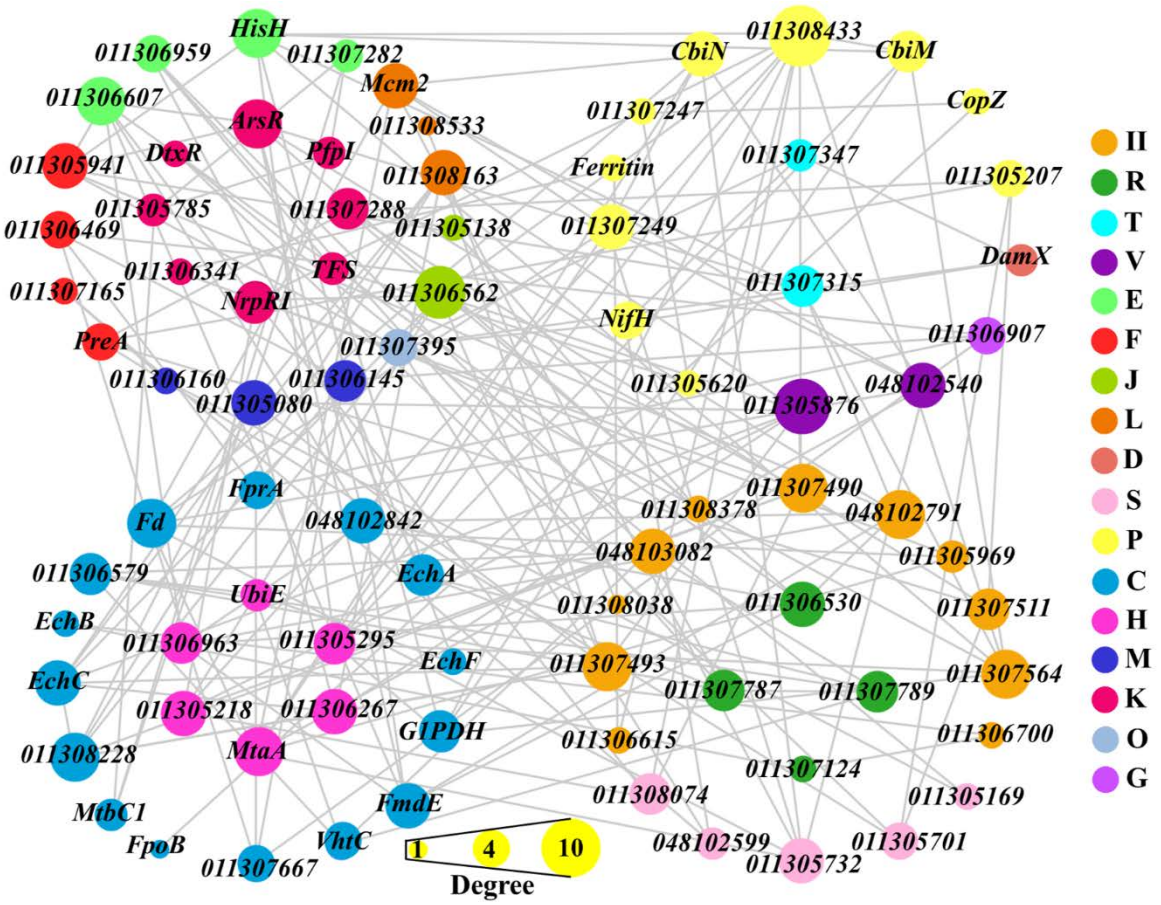

D Cell cycle control, cell division, chromosome partitioning
C Energy production and conversion
G Carbohydrate transport and metabolism
E Amino acid transport and metabolism
H Coenzyme transport and metabolism
F Nucleotide transport and metabolism
J Translation, ribosomal structure and biogenesis
K Transcription
L Replication, recombination and repair
R General function prediction only
M Cell wall/membrane/envelope biogenesis
S Function unknown
O Posttranslational modification, protein turnover, chaperones
T Signal transduction mechanisms
P Inorganic ion transport and metabolism
V Defense mechanisms
U Intracellular trafficking, secretion, and vesicular transport
II Undefinition

Fig. S20 Network analysis of the proteins with significant variations. Related to Figure 6.

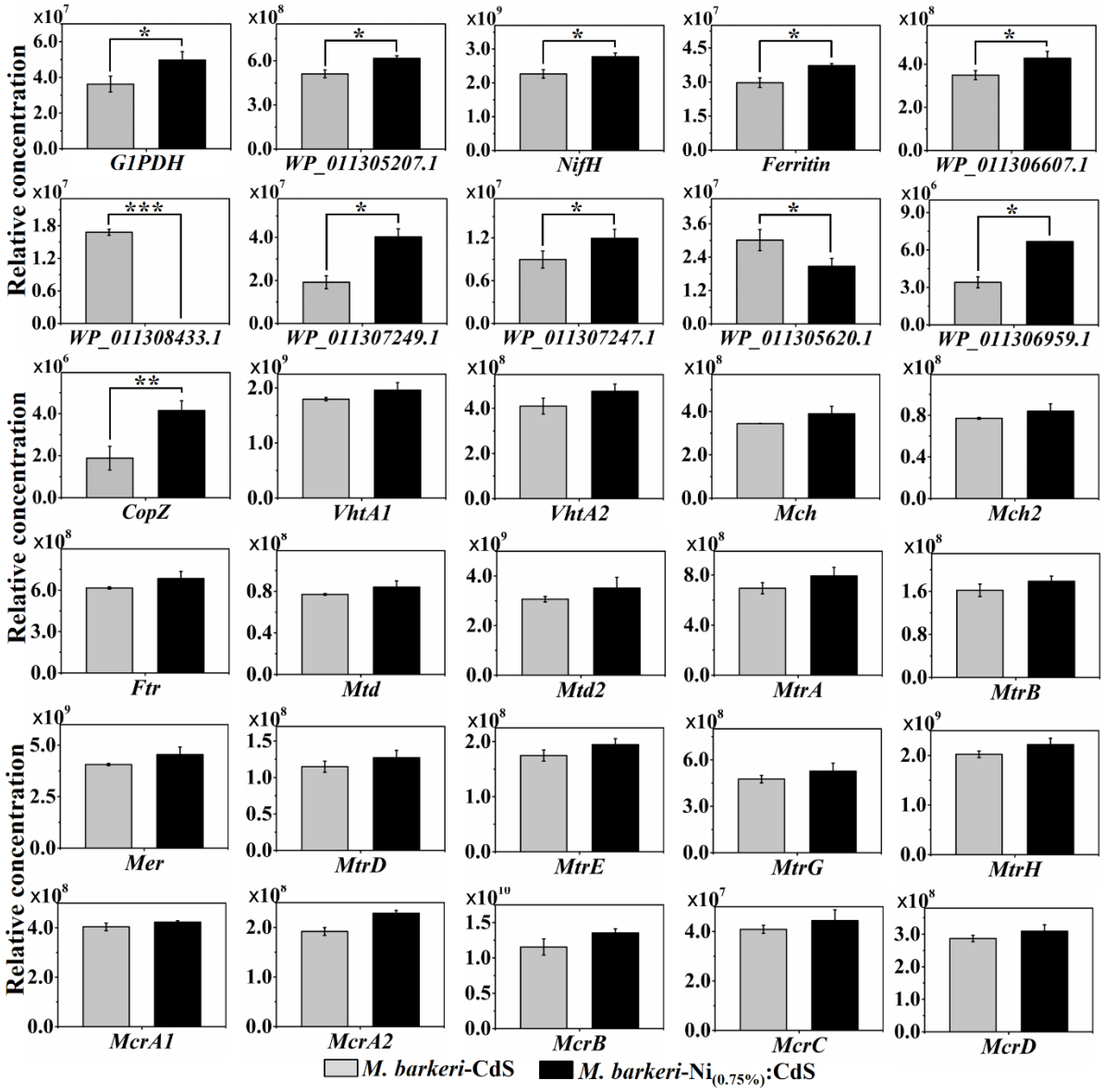

Fig. S21 Relative concentration of proteins for electron transfer, energy conversion and CO_2 fixation in *M. barkeri*-$Ni_{(0.75\%)}$:CdS biohybrids compared to *M. barkeri*-CdS biohybrids. Data are represented as mean ± SEM (n = 3). "*", "**" and "***" indicate *p* values smaller than 0.05, 0.01 and 0.001, respectively. Three biological replicates are used. Related to Figure 7.

Table S1 The composition of contained substrate medium (CSM) and uncontained substrate medium (USM). Related to Figure 2.

Component	CSM (g/L)	USM (g/L)
$MgCl_2 \cdot 6H_2O$	0.4	0.4
$CaCl_2 \cdot 2H_2O$	0.1	0.1
NH_4Cl	0.1	0.1
KH_2PO_4	0.2	0.2
KCl	0.5	0.5
HEPES	7.16	7.16
$NaHCO_3$	2.52	2.52
$Na_2S \cdot 9H_2O$	0.24	-
NaAc	1.394	-
Cysteine-HCl	-	0.24
Trace element solution SL-10*	1 mL	1 mL
Selenite-tungastate solution**	1 mL	1 mL
Vitamin solution***	3 mL	3 mL

*Per liter, the medium containing

HCl (2M)	50 mL
$FeCl_2 \cdot 4H_2O$	2 g
$ZnCl_2$	0.2 g
$MnCl_2 \cdot 4H_2O$	0.1 g
H_3BO_3	0.18 g
$CoCl_2 \cdot 6H_2O$	0.05 g
$CuCl_2 \cdot 2H_2O$	6 mg
$NiCl_2 \cdot 6H_2O$	72 mg
$Na_2MoO_4 \cdot 2H_2O$	108 mg

**Per liter, the medium containing

NaOH	0.5 g

$Na_2SeO_3 \cdot 5H_2O$	3 mg
$Na_2WO_4 \cdot 2H_2O$	4 mg

***Per liter, the medium containing

4-aminobenzoic acid	0.04 g
D(+)-biotin	0.01 g
DL-a-lipoic acid	0.01 g
Calcium-D(+)-panto-thenate	0.1 g
Pyridoxine-HCl	0.1 g
Folic acid	0.03 g
Nicotinic acid	0.05 g
Riboflavin	0.05 g
Thiamin-HCl·$2H_2O$	0.01 g
Vitamin B_{12}	0.05 g

Table S2 The photocatalytic CH_4 production performance with different biohybrids. Related to Figure 2.

Biohybrid (50 mL)	*M. barkeri* inoculum (mL)	CdS (mM)	Maximum CH_4 yield* (μmol)	Average CH_4 production rate* (μmol/h)	Light intensity (mW/cm^2)	References
M. barkeri-CdS	10	1.0	13.70	0.19	1.0	Ye et al. (2019)
M. barkeri - $Ni_{(0.75\%)}$:CdS	10	0.6	21.50	0.21	0.8	In this study
M. barkeri - $Ni_{(0.75\%)}$:CdS	10	0.6	23.04	0.24	1.0	In this study

* The value was calculated with the data that were statistically significant.

Table S3 Fit parameters for the PL decay curves of *M. barkeri*-$Ni_{(x)}$:CdS. Related to Figure 3.

	A_1	A_2	τ_1 (ns)	τ_2 (ns)	τ (ns)
M. barkeri-CdS	336.95	16.09	0.32	3.45	1.38
M. barkeri-$Ni_{(0.75\%)}$:CdS	423.16	64.24	0.80	7.00	4.32
M. barkeri-$Ni_{(2.00\%)}$:CdS	496.00	17.57	0.38	7.20	3.14

Based on the PL decay curves (Figure 3d), the parameters in Table S2 can be obtained through curve fitting. The average lifetime of the QD PL decay is calculated by using following expression:

$$\tau = \frac{\sum_n (A_n \tau_n{}^2)}{\sum_n A_n \tau_n}$$

where n corresponds to the n^{th} component of a given multi-exponential decay process (James et al., 1985).

Materials and methods

Synthesis of Ni:CdS semiconductors

The synthesis of Ni:CdS semiconductors were conducted according to the previous research (Wang et al., 2018), where 3-Mercaptopropionic acid (MPA) was used to disperse and control the particle size of CdS nanoparticles. Briefly, 5 mmol of $CdCl_2$ and 8.5 mmol of MPA were added into 100 mL of water. In addition, the Ni amount (wt. %) was varied to control the dosage volume of $NiCl_2$ to construct $Ni_{(x)}$:CdS semiconductors, where x is the nominal loading amount of Ni, which is determined by the ICP-MS measurement. For example, the addition of 10 μmol of $NiCl_2 \cdot 6H_2O$ produced 65.3 ± 0.5 mg of $Ni_{(0.75\%)}$:CdS semiconductors. Before transferring the solution into a 250 mL three-necked flask, the pH was adjusted to 10.0 by 5.0 mol/L of NaOH solution. Then, the air in the headspace of the flask was replaced with Ar, and 0.5 mmol of freshly prepared Na_2S solution was dropwise added under stirring. Subsequently, the mixture was heated to 100 ^oC with a condenser, and the observed bright-yellow, transparent solution was continually stirred at 100 ^oC for 30 min. After natural cooling to room temperature, the $Ni_{(x)}$:CdS semiconductors were isolated through precipitation with alcohol. Then, the pellet was redispersed in water and freeze dried for further use. As control, CdS semiconductors with the identical particle size were synthesized by the same method without Ni. All analytical-grade chemicals were purchased from Sigma-Aldrich and used without further purification.

Construction and characterization of *M. barkeri*-Ni:CdS biohybrid

The inoculum of *M. barkeri* (DSM 800, obtained from DSMZ, Braunschweig, Germany) was cultured in a 50-mL anaerobic heterotrophic medium at 37 ^oC (Table S1). When the growth of

M. barkeri reached an exponential phase (OD_{600}~0.2), 0.6 mmol/L $Ni_{(x)}$:CdS semiconductors were added according to the preliminary experiment, and the mixture was placed in the shaker at a speed of 180 rpm to create an *M. barkeri*-$Ni_{(x)}$:CdS biohybrid. After 3 days of cultivation, the suspension was sequentially centrifuged, washed, and resuspended in 5 mL 0.9% NaCl solution three times. As control, the *M. barkeri*-CdS biohybrid was prepared by the same method, except $Ni_{(x)}$:CdS was replaced with CdS semiconductors.

The prepared *M. barkeri*-$Ni_{(x)}$:CdS/*M. barkeri*-CdS biohybrids were collected, fixed by 4% glutaraldehyde, and sequentially dehydrated to prepare nonsectioned and thin-sectioned samples (Wang et al., 2019). Fluorescence images were collected using a Carl Zeiss LSM880 confocal laser-scanning microscope (CLSM). Micro-Raman measurement was performed using a Renishaw micro-Raman spectrometer (Tian et al., 2019). The high-resolution/transmission electron microscopy (HR-/TEM) images were obtained with a FEI Tecnai G2 F20 S-TWIN field-emission transmission electron microscope. Elemental mapping was performed by an X-MaxN energy dispersive X-ray spectrometer (EDS) attached to the TEM instrument. The X-ray diffraction (XRD) patterns were recorded with a Shimadzu XRD-6000 X-ray diffractometer. The X-ray photoelectron spectroscopy (XPS) and valence band XPS (VB XPS) experiments were conducted by a Thermo ESCALAB 250XI XPS spectrometer system.

A CHI 660E electrochemical workstation (CH Instruments Inc, Austin, TX) was used for the electrochemical measurements with 395 ± 5 nm violet LED irradiation (1.0 mW/cm^2) in a three-electrode system under N_2 gas atmosphere according to the previous research (Ye et al., 2018; Ye et al., 2019). A platinum sheet and a saturated calomel electrode (SCE) were used as the contour and reference electrodes, respectively. The thin-film working electrodes were prepared

by drop-casting 50 μL of suspensions (3 mg of semiconductors/biohybrids after dispersed in 0.5 mL of 1:3 v/v isopropyl alcohol/water solvent) onto indium tin oxide (ITO) glass substrates (1×1 cm), followed by drying the film overnight. A 100 mM phosphate buffer solution (PBS) (pH = 7) was used as the electrolyte solution (prepared with 0.13 g/L KCl, 5.93 g/L $NaH_2PO_4 \cdot 2H_2O$ and 22.2 g/L $Na_2HPO_4 \cdot 12H_2O$). The photocurrent (*I-t*) was measured by light irradiation (light on/off cycles: 20 s) at a bias potential of -0.4 V (vs. SCE). The square wave voltammetry (SWV) between -0.6 and 0 V (vs. SHE) was performed with a scan rate of 2 mV/s. The electrochemical impedance spectroscopy (EIS) analyses were conducted in a frequency range of 1×10^5 to 0.1 Hz with a sinusoidal perturbation amplitude of 5 mV. Linear sweep voltammetry (LSV) was operated from 0.3 to -1.5 V (vs. SCE) with a scan rate of 2 mV/s in an aqueous solution. A glassy carbon electrode (3 mm in diameter) was used as the working electrode, and the samples were loaded by transferring the catalyst dispersion (3 mg of biohybrids, 50 μL of 5 wt% Nafion solution, and 1.0 mL of ethanol solvent) onto the glassy carbon, followed by drying the film overnight. Steady-state photoluminescence (PL) spectra and PL decay spectra were determined on the FLS980 photoluminescence spectrometer. The lifetime data were analyzed with DataStation V6.6 (Horiba Scientific). The ultraviolet/visible (UV-vis) diffused reflectance spectra and UV-vis absorption spectra were recorded on a Shimadzu UV2600 UV spectrometer.

As indicative of biomass growth, the total protein content of *M. barkeri* was analyzed following a previously reported method (Pushpakumari Kudahettige et al., 2018). Membrane-bound proteins of *M. barkeri* were mechanically isolated as described (Mehta et al., 2005), and measured with the BCA Protein Assay Kit (Thermo Scientific Pierce). The concentrations of

Cd and Ni elements in the membrane-bound protein of *M. barkeri* were quantified with a NexION 300X inductively coupled plasma mass spectrometer. The NADH/NAD ratio of *M. barkeri* was measured with the Sigma-Aldrich NADH/NAD quantification kit (MAK 037). The number of cells in different samples was measured by flow cytometry (Quanta SC, Beckman Coulter) according to Xiao et al. (2017).

Photocatalytic CO_2-to-CH_4 conversion experiments

The photocatalytic CO_2-to-CH_4 conversion experiments were conducted in 125-mL serum bottles with 50-mL sterilized autotrophic medium (pH = 6.8, Table S1). After flushing the bottles with CO_2:N_2 (80:20) for 30 min, 5 mL *M. barkeri*-$Ni_{(x)}$:CdS suspension and cysteine at 0.15 wt% (sacrificial agent) were added. Then, the bottles were placed in a constant temperature incubator to maintain at 35 ± 2 ^oC, and irradiated by a visible-light source. The 395 ± 5 nm violet LEDs and 300 W Xenon lamp (CEL-HXF300, Ceaulight, China) with a 400 nm filter were employed as the visible-light source. Parallel studies were conducted, Where *M. barkeri*, $Ni_{(x)}$:CdS, and light were removed or replaced by CdS semiconductors, while 0.15 wt% cysteine was still added. The CH_4 concentration was determined by a Shimadzu GC2014 gas chromatograph. Moreover, the isotope-labeled experiments were conducted using $NaH^{13}CO_3$ instead of $NaH^{12}CO_3$ in the medium. Then, the products were measured with an Agilent 7890-5975c gas chromatography-mass spectrometer (GC-MS). The average quantum yield (*QE*) was calculated according to previous research (Sakimoto et al., 2016). The photosynthetic CH_4 efficiencies of *M. barkeri*-$Ni_{(0.75\%)}$:CdS biohybrids could also be calculated based on the initial Cys concentration according to Eq. S1. The 0.15 wt% Cys·HCl (MW = 157.62 $g \cdot mol^{-1}$) in the photosynthesis measurements, corresponds to 457.83 μmol Cys. With the above stoichiometry,

this leads to a maximum CH_4 production yield of 57.23 μmol. Then the quantum yield based on the initial Cys concentration is defined as:

$$\text{Quantum yield}(\%) = \frac{n_{CH_4}}{57.23} \times 100\% \quad \text{(S1)}$$

where n_{CH_4} is the CH_4 yield.

Density functional theory (DFT) theoretical calculation

Three greenockite models were established with different numbers of Ni atoms in the 8 atom cells, which are named Cd_4S_4, $Cd_3Ni_1S_4$, and $Cd_2Ni_2S_4$. Their electronic structures were investigated via the plane-wave-pseudopotential approach based on the density functional theory. For the original model, we determined the stability of the doped structure before calculating the electronic structures. The convergence tolerances for the energy, maximum force, maximum stress, maximum displacement were set to 5.0×10^{-6} eV/atom, 0.01 eV/Å, 0.02 GPa, 5.0×10^{-4} Å, respectively. The electronic exchange-correlation energy was calculated with Perdew-Burke-Ernzerhof (PBE) of the generalized gradient approximation. The electron-core interaction was using norm conserving pseudopotentials with a plane-wave basis cutoff energy of 290 eV. The self-consistent field tolerance was 5.0×10^{-6} eV/atom. The FFT grids and augmentation density scaling factor of all models were $36\times36\times36$ and 1.5, respectively. The k-points were set to $4\times4\times4$ for all optimized models.

References

James, D. R., Liu, Y. S., Mayo, P. De, Ware, W. R. (1985). Distributions of fluorescence lifetimes: consequences for the photophysics of molecules adsorbed on surfaces. *Chem. Phys. Lett. 120*, 460-465.

Mehta, T., Coppi, M. V., Childers, S. E., Lovley. D. R. (2005). Outer membrane c-type cytochromes required for Fe (III) and Mn (IV) oxide reduction in *Geobacter sulfurreducens*. Appl. Environ. Microbiol. *71*, 8634-8641.

Meng, X., Wang, T., Liu, L., Ouyang, S., Li, P., Hu, H., Kako, T., Iwai, H., Tanaka, A., Ye, J. (2014). Photothermal conversion of CO_2 into CH_4 with H_2 over Group VIII nanocatalysts: an alternative approach for solar fuel production. Angew. Chem. Int. Edit. *53*, 11478-11482.

Pei, L., Li, T., Yuan, Y., Yang, T., Zhong, J., Ji, Z., Yan, S., Zou, Z. (2019). Schottky junction effect enhanced plasmonic photocatalysis by TaON@ Ni NP heterostructures. Chem. Commun. *55*, 11754-11757.

Pushpakumari Kudahettige, N., Pickova, J., Gentili, F. G. (2018). Stressing algae for biofuel production: Biomass and biochemical composition of *Scenedesmus dimorphus* and *Selenastrum minutum* grown in municipal untreated wastewater. Front. Energ. Res. *6*, 132.

Sakimoto, K. K., Wong, A. B., Yang, P. (2016). Self-photosensitization of nonphotosynthetic bacteria for solar-to-chemical production. Science *351*, 74-77.

Tian, L. J., Min, Y., Li, W. W., Chen, J. J., Zhou, N. Q., Zhu, T. T., Li, D. B., Ma, J. Y., An, P. F., Zheng, L. R., Huang, H., Liu, Y. Z., Yu, H. Q. (2019). Substrate metabolism-driven assembly of high-quality CdS_xSe_{1-x} quantum dots in *Escherichia coli*: Molecular mechanisms and bioimaging application. ACS Nano *13*, 5841-5851.

Wang, B., Xiao, K., Jiang, Z., Wang, J., Jimmy, C. Y., Wong, P. K. (2019). Biohybrid photoheterotrophic metabolism for significant enhancement of biological nitrogen fixation in pure microbial cultures. Energ. Environ. Sci. *12*, 2185-2191.

Wang, J., Xia, T., Wang, L., Zheng, X. S., Qi, Z. M., Gao, C., Zhu, J. F., Li, Z. Q., Xu, H. X., Xiong, Y. J. (2018). Enabling visible−light−driven selective CO_2 reduction by doping quantum dots: Trapping electrons and suppressing H_2 evolution. Angew. Chem. Int. Edit. *57*, 16447-16451.

Xiao, Y., Zhang, E., Zhang, J., Dai, Y., Yang, Z., Christensen, H. E., Ulstrup, J., Zhao, F. (2017). Extracellular polymeric substances are transient media for microbial extracellular electron transfer. Sci. Adv. *3*, e1700623.

Ye, J., Hu, A. D., Ren, G. P., Chen, M., Tang, J. H., Zhang, P. Y., Zhou, S. G., He, Z. (2018). Enhancing sludge methanogenesis with improved redox activity of extracellular polymeric substances by hematite in red mud. Water Res. *134*, 54-62.

Ye, J., Yu, J., Zhang, Y. Y., Chen, M., Liu, X., Zhou, S., He, Z. (2019). Light-driven carbon dioxide reduction to methane by *Methanosarcina barkeri*-CdS biohybrid. Appl. Catal. B-Environ. *257*, 117916.